ARTICLE NO. 78-1208R

Geometric Conservation Law and Its Application to Flow Computations on Moving Grids

P. D. Thomas* and C. K. Lombard†
Lockheed Palo Alto Research Laboratory, Palo Alto, Calif.

Boundary-conforming coordinate transformations are used widely to map a flow region onto a computational space in which a finite-difference solution to the differential flow conservation laws is carried out. This method entails difficulties with maintenance of global conservation and with computation of the local volume element under time-dependent mappings that result from boundary motion. To improve the method, a differential "geometric conservation law" (GCL) is formulated that governs the spatial volume element under an arbitrary mapping. The GCL is solved numerically along with the flow conservation laws using conservative difference operators. Numerical results are presented for implicit solutions of the unsteady Navier-Stokes equations and for explicit solutions of the steady supersonic flow equations.

I. Introduction

BOTH finite-difference methods[1-4] and finite-volume methods[5-7] have been used to solve the gasdynamic equations written in the form of mass, momentum, and energy conservation laws. The two methods are based on differential and integral statements of these laws, respectively. To illustrate the methods, consider the integral statement of the law of mass conservation for a spatial region R of volume $\mathcal{V}$ bounded by a closed surface S.

$$\frac{\mathrm{d}}{\mathrm{d}t}\int_{\mathcal{V}} \rho \mathrm{d}\mathcal{V} + \int_S \rho(\boldsymbol{V}-\boldsymbol{W}_s)\cdot \mathrm{d}\boldsymbol{S} = 0 \tag{1}$$

where ρ is the density, $\boldsymbol{V}$ is the fluid velocity, and $\boldsymbol{W}_s$ denotes the local velocity of the boundary surface S.

In the finite-volume method, the region R is subdivided into a network consisting of a fixed number of contiguous cells of volume $\Delta\mathcal{V}_i$ bounded by cell faces S_{ij}. Equation (1) is applied to each cell individually to obtain

$$\frac{\mathrm{d}}{\mathrm{d}t}\int_{\Delta\mathcal{V}_i} \rho \mathrm{d}\mathcal{V} + \sum_j \int_{S_{ij}} \rho(\boldsymbol{V}-\boldsymbol{W}_s)\cdot \mathrm{d}\boldsymbol{S} = 0 \tag{2}$$

Geometrical relations are used to construct cell volumes $\Delta\mathcal{V}_i$ and cell face areas S_{ij} for each cell at each instant in time. Once the cell areas and volumes are constructed, Eq. (2) is solved by some numerical time-integration scheme to determine the time variation of the cell-averaged density:

$$\bar{\rho}_i = \int_{\Delta\mathcal{V}_i} \rho \mathrm{d}\mathcal{V} \Big/ \int_{\Delta\mathcal{V}_i} \mathrm{d}\mathcal{V} \tag{3}$$

For later reference, we emphasize two obvious facts about the described method. First, the process of geometrically constructing cell volumes $\Delta\mathcal{V}_i$ and cell face areas S_{ij} is equivalent to solving numerically the following integral statement of the relation that determines the time variation of the cell volume in terms of the areas, orientations, and velocities of the cell faces

$$\frac{\mathrm{d}}{\mathrm{d}t}\int_{\Delta\mathcal{V}_i} \mathrm{d}\mathcal{V} = \sum_j \int_{S_{ij}} \boldsymbol{W}_s \cdot \mathrm{d}\boldsymbol{S}$$

The corresponding global statement for the entire region R is

$$\frac{\mathrm{d}}{\mathrm{d}t}\int_{\mathcal{V}} \mathrm{d}\mathcal{V} = \int_S \boldsymbol{W}_s \cdot \mathrm{d}\boldsymbol{S} \tag{4}$$

We call this last equation the integral form of the "geometric conservation law" (GCL) because it deals with geometric properties of R and has the same general form as the integral statement in Eq. (1) of the mass conservation law. Second, the network of cells whose motion is tied by construction to that of the boundary surface S can be viewed as the discrete representation of a mapping from the coordinate system in which the basic Eq. (1) is written to a new boundary-conforming coordinate system, since each peripheral cell has a face that coincides with a part of the boundary surface S for all time.

The differential statement of the mass conservation law

$$\rho_t + \nabla\cdot\rho\boldsymbol{V} = 0 \tag{5}$$

is obtained from the integral statement in Eq. (1) by using the divergence theorem to transform the surface integral into a volume integral.

In the finite-difference method, one starts with Eq. (5) in some selected coordinate system. A mapping is introduced directly that transforms the spatial and temporal independent variables to a boundary-conforming curvilinear coordinate system in which the boundary surface S is a coordinate surface.[1-4,8] This coordinate transformation adds extra terms to Eq. (5) and introduces the transformation Jacobian J, as a coefficient multiplying the density inside the time-derivative term.[4,9] The region R then is covered by a grid consisting of a fixed number of nodal points distributed over R and along its bounding surface. The transformed counterpart of Eq. (5) is discretized to arrive at difference equations governing the time variation of the product $J\rho$ at each node of the grid. Then

Presented as Paper 78-1208 at the AIAA 11th Fluid and Plasma Dynamics Conference, Seattle, Wash., July 10-12, 1978; submitted July 27, 1978; revision received March 12, 1979.

Index categories: Computational Methods; Viscous Nonboundary-Layer Flows; Supersonic and Hypersonic Flow.

*Staff Scientist, Applied Mechanics Lab. Member AIAA.

†Research Scientist, Applied Mechanics Lab. Presently with Pacific Engineering Design and Analysis Co., Palo Alto, Calif. Member AIAA.

J must be known before ρ can be calculated. Because J represents the volume element in the transformed coordinate system, this approach implies the existence of an effective volume element $\Delta\mathcal{V}$ associated with each grid point. The numerical value of $\Delta\mathcal{V}$ is indirectly determined by the difference scheme that is used to discretize Eq. (5). Clearly, the numerical value of J that one uses to compute ρ must be consistent with the value of $\Delta\mathcal{V}$ implied by the difference scheme, or the solution ρ will be in error. This fact apparently has not been recognized previously by finite-difference practitioners. Arbitrary procedures are commonly employed to compute the effective value of J at each grid point. For time-varying grids, such procedures generate errors because they generally are inconsistent with the actual effect of the differencing scheme on the effective volume element inherent in the transformed flow equations.

A further distinction between finite-difference and finite-volume methods lies in their ability to preserve faithfully the global conservation properties that are inherent in the mathematical statements of the flow conservation laws, as distinct from the numerical representation of those laws by either numerical method. For example, the global mass conservation relation (1) is preserved in the finite-volume method simply by defining a unique value in Eq. (2) for the mass flux $\rho(\boldsymbol{V}-\boldsymbol{W}_s)\cdot d\boldsymbol{S}$ passing through the face S common to two contiguous cells. Global mass conservation is preserved by the finite-difference method only if "conservative" spatial difference operators are employed in the finite-difference representation of Eq. (5).

We have discovered that it is possible to formulate a differential statement of the GCL corresponding to the integral statement in Eq. (4). The differential GCL is similar in form to the differential flow conservation laws, and governs the time variation of the Jacobian J. If the differential GCL is solved numerically with the same finite-difference scheme that is used to integrate the flow conservation laws, it yields a self-consistent solution for the effective volume element associated with each grid point. For interior grid points, this improved finite-difference method is equivalent to the finite-volume method, but is easier to apply because no external geometrical constructions are needed to compute either cell volumes or surface areas and spatial orientations of cell faces. We shall refer to the improved finite-difference method based on the differential GCL as the "modified finite-volume method."

II. Differential Statement of the Geometric Conservation Law

Cartesian Coordinates

The basis for the modified finite-volume method is the differential GCL. We now illustrate how the latter is derived from the integral form in Eq. (4) for a spatial region R and boundary surface S specified initially in Cartesian coordinates x,y,z. We introduce a time-dependent invertible mapping transformation of R onto boundary-conforming curvilinear coordinates.[4,8,9]

$$x,y,z,t \underset{T^{-1}}{\overset{T}{\rightleftharpoons}} \xi,\eta,\zeta,\tau \qquad \begin{aligned} \xi &= \xi(x,y,z,t) \\ \eta &= \eta(x,y,z,t) \\ \zeta &= \zeta(x,y,z,t) \\ \tau &= t \end{aligned} \tag{6}$$

Here, the precise meaning of the term "boundary-conforming" is that, in these coordinates, the boundary S is composed only of segments of coordinate surfaces $\xi=\text{const}$, $\eta=\text{const}$, $\zeta=\text{const}$. That is, the surface S has the time-invariant functional representation $f(\xi,\eta,\zeta)=0$ independently of time τ.

In the Cartesian coordinate system, the velocity of any point on S can be written in terms of its x, y, and z components as

$$\boldsymbol{W}_s=(x_\tau,y_\tau,z_\tau) \quad \text{for} \quad (x,y,z)\epsilon S \tag{7}$$

The mapping defines a vector field

$$\boldsymbol{W}=(x_\tau,y_\tau,z_\tau) \tag{8}$$

throughout the region R that coincides with $\boldsymbol{W}_s$ on the boundary. This allows us to apply the divergence theorem to replace the surface integral on the right side of Eq. (4) by a volume integral. When the volume integrals are transfomed to the ξ,η,ζ coordinate system, there results

$$\frac{d}{dt}\int_{\mathcal{V}} J d\xi d\eta d\zeta = \int_{\mathcal{V}} (\nabla\cdot\boldsymbol{W}) J d\xi d\eta d\zeta \tag{9}$$

where the volume is $d\mathcal{V}=dx\,dy\,dz=J\,d\xi\,d\eta\,d\zeta$ and J is the Jacobian of the inverse transformation T^{-1}

$$J=\frac{\partial(x,y,z)}{\partial(\xi,\eta,\zeta)} \tag{10}$$

Because ξ, η, ζ were constructed as boundary-conforming coordinates in which both S and its enclosed volume $\mathcal{V}$ are fixed in time τ, the time derivative operator on the left side of Eq. (9) may be moved inside the integral.

Upon expanding the integral on the right-hand side of Eq. (9) as follows

$$\begin{aligned} J\nabla\cdot\boldsymbol{W} &= J(\nabla\xi\cdot\boldsymbol{W}_\xi+\nabla\eta\cdot\boldsymbol{W}_\eta+\nabla\zeta\cdot\boldsymbol{W}_\zeta) \\ &= (J\nabla\xi\cdot\boldsymbol{W})_\xi+(J\nabla\eta\cdot\boldsymbol{W})_\eta+(J\nabla\zeta\cdot\boldsymbol{W})_\zeta \\ &\quad -\boldsymbol{W}\cdot[(J\nabla\xi)_\xi+(J\nabla\eta)_\eta+(J\nabla\zeta)_\zeta] \end{aligned}$$

and making use of the identities

$$\xi_t=-\nabla\xi\cdot\boldsymbol{W} \quad \eta_t=-\nabla\eta\cdot\boldsymbol{W} \quad \zeta_t=-\nabla\zeta\cdot\boldsymbol{W}$$

the results can be written in the form

$$\begin{aligned} \int_{\mathcal{V}} [J_\tau+\hat{\xi}_{t\xi}+\hat{\eta}_{t\eta}+\hat{\zeta}_{t\zeta}]d\xi\,d\eta\,d\zeta &= \int_{\mathcal{V}} [x_\tau(\hat{\xi}_{x\xi}+\hat{\eta}_{x\eta}+\hat{\zeta}_{x\zeta}) \\ &\quad +y_\tau(\hat{\xi}_{y\xi}+\hat{\eta}_{y\eta}+\hat{\zeta}_{y\zeta})+z_\tau(\hat{\xi}_{z\xi}+\hat{\eta}_{z\eta}+\hat{\zeta}_{z\zeta})]d\xi\,d\eta\,d\zeta \end{aligned} \tag{11}$$

where

$$\hat{\xi}_t=J\xi_t, \quad \hat{\xi}_x=J\xi_x, \quad \hat{\xi}_y=J\xi_y, \quad \text{etc.}$$

One can verify by a direct calculation that each expression in parentheses on the right-hand side of Eq. (11) vanishes identically if the mapping functions are sufficiently differentiable. Since $\mathcal{V}$ is fixed in τ, Eq. (11) reduces to the following differential statement of the GCL

$$J_\tau+(\hat{\xi}_t)_\xi+(\hat{\eta}_t)_\eta+(\hat{\zeta}_t)_\zeta=0 \tag{12}$$

This simple partial differential equation bears a close resemblance to the transformed flow conservation equations. For example, the strong conservation-law form of the Navier-Stokes equations in Cartesian coordinates can be written as

$$q_t+f_x+g_y+h_z=\sigma_x+\theta_y+\omega_z \tag{13}$$

$$q=(\rho,\ \rho u,\ \rho v,\ \rho w,\ \rho E)^T$$

$$f=(\rho u,\ p+\rho u^2,\ \rho uv,\ \rho uw,\ \rho uH)^T$$

$$E=e+(u^2+v^2+w^2)/2$$

$$\boldsymbol{g}=(\rho v,\ \rho vu,\ p+\rho v^2,\ \rho vw,\ \rho vH)^T \qquad H=E+p/\rho$$

$$\boldsymbol{h}=(\rho w,\ \rho wu,\ \rho wv,\ p+\rho w^2,\ \rho wH)^T$$

where u, v, w, are the velocity components in the coordinate directions x, y, z; ρ is the density, p the pressure, e the specific internal energy; and σ, θ, ω represent the viscous stress and work terms for each coordinate direction. Upon transforming to ξ, η, ζ coordinates with the aid of the chain rule for partial derivatives, Eq. (13) becomes[9,14]

$$\hat{q}_\tau+\hat{f}_\xi+\hat{g}_\eta+\hat{h}_\zeta=\hat{\sigma}_\xi+\hat{\theta}_\eta+\hat{\omega}_\zeta \tag{14}$$

$$\hat{q}=Jq$$

$$\hat{f}=\hat{\xi}_t q+\hat{\xi}_x f+\hat{\xi}_y g+\hat{\xi}_z h \qquad \hat{\sigma}=\hat{\xi}_x\sigma+\hat{\xi}_y\theta+\hat{\xi}_z\omega$$

$$\hat{g}=\hat{\eta}_t q+\hat{\eta}_x f+\hat{\eta}_y g+\hat{\eta}_z h \qquad \hat{\theta}=\hat{\eta}_x\sigma+\hat{\eta}_y\theta+\hat{\eta}_z\omega$$

$$\hat{h}=\hat{\zeta}_t q+\hat{\zeta}_x f+\hat{\zeta}_y g+\hat{\zeta}_z h \qquad \hat{\omega}=\hat{\zeta}_x\sigma+\hat{\zeta}_y\theta+\hat{\zeta}_z\omega$$

One can see that the geometric conservation law, Eq. (12), has the same form as the flow conservation laws, Eq. (14). In face, the GCL can be deduced directly from the mass conservation equation [the first component of the vector Eq. (14)] by setting $\rho=1$, $V=0$. The same is true of the integral form in Eqs. (1) and (4).

In problems where some part of the surface S bounding the physical flow region R moves in time, the boundary-conforming character of the mapping transformation implies a corresponding motion of all grid points in physical space. This grid motion can induce errors in the computed flowfield unless Eq. (12) is satisfied numerically by the difference scheme. We conjecture that such grid motion-induced errors are responsible for the oscillations and instabilities encountered by Viviand and Ghazzi[3] in solving Eq. (14) on a moving grid. This would explain why those authors found that the instabilities disappeared when they abandoned the conservative Eq. (14) in favor of the nonconservative formulation that involves q_τ rather than $(Jq)_\tau$.

In general, the simplest way to avoid grid motion-induced errors in solving the flow conservation laws of Eq. (14) with a particular differencing scheme is to solve Eq. (12) with the same scheme. This procedure insures a self-consistent solution for the effective volume element associated with each nodal point of a dynamic grid. The numerical solution of the GCL in Eq. (12) requires no boundary conditions, but only initial conditions that can be computed from the geometric definition of the Jacobian

$$J=\hat{\xi}_x x_\xi+\hat{\xi}_y y_\xi+\hat{\xi}_z z_\xi$$

Cylindrical Coordinates

The modified finite-volume method based on the GCL can be formulated for non-Cartesian base coordinate systems. It can also be applied to steady, inviscid, supersonic flows where there exists a timelike spatial coordinate with respect to which the flow equations are hyperbolic. As an example, we consider three-dimensional flows in which the velocity component w in the direction of the axis of a cylindrical coordinate system (r,ϕ,z) is everywhere supersonic.

It is possible to express the equations in strong conservation form, with the exception of the radial momentum equation, which contains an inhomogeneous term that cannot be avoided.[16] For adiabatic flow ($H=$const), the equations are

$$\boldsymbol{a}_z+\boldsymbol{c}_r+\boldsymbol{d}_\phi-\boldsymbol{e}=0 \tag{15}$$

where

$$\boldsymbol{a}=r(\rho w,\ \rho uw,\ r\rho vw,\ p+\rho w^2)^T$$

$$\boldsymbol{c}=r(\rho u,\ p+\rho u^2,\ r\rho vu,\ \rho wu)^T$$

$$\boldsymbol{d}=[\rho v,\ \rho uv,\ r(p+\rho v^2),\ \rho vw]^T$$

$$\boldsymbol{e}=(0,\ p+\rho v^2,\ 0,\ 0)^T$$

Under the general boundary-conforming coordinate transformation

$$r,\phi,z\rightarrow X,\ Y,\ Z \qquad \begin{aligned} X&=X(r,\phi,z)\\ Y&=Y(r,\phi,z)\\ Z&=z\end{aligned}$$

the equations assume the form

$$\hat{\boldsymbol{a}}_Z+\hat{\boldsymbol{c}}_X+\hat{\boldsymbol{d}}_Y-\hat{\boldsymbol{e}}=0 \tag{16}$$

where

$$\hat{\boldsymbol{a}}=J\boldsymbol{a} \quad \hat{\boldsymbol{e}}=J\boldsymbol{e}=(r_X\phi_Y-r_Y\phi_X)\boldsymbol{e}$$

$$\hat{\boldsymbol{c}}=\hat{X}_z\boldsymbol{a}+\hat{X}_r\boldsymbol{c}+\hat{X}_\phi\boldsymbol{d} \quad \hat{\boldsymbol{d}}=\hat{Y}_z\boldsymbol{a}+\hat{Y}_r\boldsymbol{c}+\hat{Y}_\phi\boldsymbol{d}$$

$$\hat{X}_z=r_Y\phi_Z-r_Z\phi_Y \quad \hat{X}_r=\phi_Y \quad \hat{X}_\phi=-r_Y$$

$$\hat{Y}_z=r_X\phi_Z-r_Z\phi_X \quad \hat{Y}_r=-\phi_X \quad \hat{Y}_\phi=r_X \tag{17}$$

The axial coordinate z is a timelike coordinate and the integral statement of the geometric conservation law is

$$\frac{\mathrm{d}}{\mathrm{d}z}\int_A \mathrm{d}A=\int_S \boldsymbol{W}\cdot\mathrm{d}\boldsymbol{S}=\int_A (\nabla\cdot\boldsymbol{W})\mathrm{d}A$$

where $\mathrm{d}A=r\ \mathrm{d}r\ \mathrm{d}\phi=rJ\ \mathrm{d}X\ \mathrm{d}Y$ is the element of area in a plane $z=$const and S is the boundary curve in that plane. The analog of the boundary velocity in Eq. (8) is

$$\boldsymbol{W}=r_Z\boldsymbol{e}_r+r\phi_Z\boldsymbol{e}_\phi$$

where $\boldsymbol{e}_r$, $\boldsymbol{e}_\phi$ are the unit vectors of the polar coordinate system in a $z=$const plane. Upon expanding the divergence $\nabla\cdot\boldsymbol{W}$ in polar coordinates and performing some straightforward algebraic manipulations, we obtain the following differential statement of the GCL

$$(rJ)_Z+(r\hat{X}_z)_X+(r\hat{Y}_z)_Y=0 \tag{18}$$

This last equation governs the axial variation of the quantity rJ that appears as a scale factor in the first term of the vector Eq. (16). If the same finite-difference scheme is used to solve both Eqs. (16) and (18), the computed value of rJ will always be properly "centered" in the r, ϕ grid at each Z step of the integration. However, an additional GCL is required for the ϕ momentum equation [third component of the vector Eq. (16)] because the dependent variable in that equation is weighted by the factor r^2. One can easily show that the appropriate GCL is identical in form to Eq. (18), but with the factor r replaced by r^2. In the following sections, the modified finite-volume method based on the GCL is developed further for both implicit and explicit difference schemes and is applied to several viscous and inviscid flow problems.

III. Implicit Solutions to the Navier-Stokes Equations

Formulation

The schemes developed by Beam and Warming[12] and by Briley and MacDonald[13] are basically similar in their use of implicit time differencing and of alternating direction techniques (operator factorization) for the multidimensional Navier-Stokes equations. The Beam-Warming scheme was combined with the general mapping in Eq. (6) by Steger[4] for two-dimensional plane flow, by Kutler et al.[2] for axisymmetric flow, an by Pulliam and Steger[14] for three-dimensional flow. We now show how the latter formulation of the implicit scheme must be modified to make use of the GCL.

The mapping function in Eq. (6) need not be known analytically. The inverse transformation T^{-1} can be defined numerically in terms of the Cartesian coordinates $x(\tau)$, $y(\tau)$, $z(\tau)$ of the grid points, from which the partial derivatives x_τ, y_τ, x_ξ, y_ξ, etc., are computed by using difference formulas. The coefficients that appear in Eqs. (12) and (14) then can be evaluated from the following identities (see Pulliam and Steger,[14] who use J to denote the Jacobian of T rather than of T^{-1}).

$$\begin{aligned}
&\hat{\xi}_x = y_\eta z_\zeta - y_\zeta z_\eta \qquad && \hat{\eta}_x = y_\zeta z_\xi - y_\xi z_\zeta \\
&\hat{\xi}_y = z_\eta x_\zeta - z_\zeta x_\eta && \hat{\eta}_y = z_\zeta x_\xi - z_\xi x_\zeta \\
&\hat{\xi}_z = x_\eta y_\zeta - x_\zeta y_\eta && \hat{\eta}_z = x_\zeta y_\xi - x_\xi y_\zeta \\
&\hat{\zeta}_x = y_\xi z_\eta - y_\eta z_\xi && \hat{\xi}_t = -(\hat{\xi}_x x_\tau + \hat{\xi}_y y_\tau + \hat{\xi}_z z_\tau) \\
&\hat{\zeta}_y = z_\xi x_\eta - z_\eta x_\xi && \hat{\eta}_t = -(\hat{\eta}_x x_\tau + \hat{\eta}_y y_\tau + \hat{\eta}_z z_\tau) \\
&\hat{\zeta}_z = x_\xi y_\eta - x_\eta y_\xi && \hat{\zeta}_t = -(\hat{\zeta}_x x_\tau + \hat{\zeta}_y y_\tau + \hat{\zeta}_z z_\tau)
\end{aligned} \tag{19}$$

For the moment, we restrict attention to inviscid flow ($\sigma = \theta = \omega = 0$) and to simple implicit-Euler time differencing of Eq. (14).

$$\Delta\hat{q} + \Delta\tau(\hat{f}_\xi + \hat{g}_\eta + \hat{h}_\zeta)^{n+1} = 0 \tag{20}$$

where Δ denotes the forward time-difference operator and the superscript denotes the time level.

If the boundary velocity in Eq. (7) is specified a priori, then the grid point velocities are known from Eq. (8) and the grid point coordinates at the advanced time can be computed explicitly within the first-order time-accuracy of Eq. (20)

$$x^{n+1} = x^n + (\Delta\tau)x_\tau^n \tag{21}$$

and similarly for y^{n+1}, z^{n+1}. The metric coefficients $\hat{\xi}_t^{n+1}$, $\hat{\xi}_x^{n+1}$, etc., that appear in $\hat{f}^{n+1}$, $\hat{g}^{n+1}$, $\hat{h}^{n+1}$ follow directly from Eq. (19), and the time-differenced form of the GCL [Eq. (12)] becomes a completely explicit difference equation for the Jacobian

$$\Delta J = -\Delta\tau[(\hat{\xi}_t)_\xi^{n+1} + (\hat{\eta}_t)_\eta^{n+1} + (\hat{\zeta}_t)_\zeta^{n+1}] \tag{22}$$

We now rewrite the first term in Eq. (20) using the identity

$$\Delta\hat{q} = q^n\Delta J + J^{n+1}\Delta q$$

and time linearize the resulting equation to obtain the following expression, which is written in the operator notation introduced by Steger[4]

$$[J^{n+1}I + \Delta\tau(\partial_\xi\hat{F} + \partial_\eta\hat{G} + \partial_\zeta\hat{H})]\Delta q = -r \tag{23a}$$

$$\hat{F} = \hat{\xi}_t^{n+1}I + \hat{\xi}_x^{n+1}F^n + \hat{\xi}_y^{n+1}G^n + \hat{\xi}_z^{n+1}H^n \tag{23b}$$

$$r = q^n\Delta J + \Delta\tau(\partial_\xi\hat{f} + \partial_\eta\hat{g} + \partial_\zeta\hat{h}) \tag{23c}$$

$$\hat{f} = \hat{\xi}_t^{n+1}q^n + \hat{\xi}_x^{n+1}f^n + \hat{\xi}_y^{n+1}g^n + \hat{\xi}_z^{n+1}h^n \tag{23d}$$

where I is the identity matrix; $F = \partial f/\partial q$, $G = \partial g/\partial q$, $H = \partial h/\partial q$ are the Jacobian matrices; and the expressions that define the matrix $\hat{G}$ and the vector $\hat{g}$ can be obtained from Eqs. (23b) and (23d), respectively, by the substituion $\xi \to \eta$. The matrix $\hat{H}$ and the vector $\hat{h}$ are defined similarly by the substitution $\xi \to \zeta$.

Upon factoring the implicit operator in Eq. (23a) we obtain the ADI sequence

$$(IJ^{n+1} + \Delta\tau\partial_\xi\hat{F})\Delta q^{**} = -r \tag{24a}$$

$$(IJ^{n+1} + \Delta\tau\partial_\eta\hat{G})\Delta q^{*} = IJ^{n+1}\Delta q^{**} \tag{24b}$$

$$(IJ^{n+1} + \Delta\tau\partial_\zeta\hat{H})\Delta q = IJ^{n+1}\Delta q^{*} \tag{24c}$$

The preceding formulation may be extended readily to include the viscous terms[14] or to employ second-order time differencing.[12] For a stationary grid, ($x_\tau = y_\tau = z_\tau = 0$), Eq. (24) is equivalent to that employed by Pulliam and Steger.[14] For a moving grid, the present scheme differs in that J^{n+1} is computed from the discretized GCL in Eq. (22) and the sequence in Eq. (24) yields Δq directly.

We now demonstrate that use of the GCL is essential for moving grids, because the grid motion induces errors in the computed flow variables unless the GCL is satisfied numerically. If one were to start initially with a spatially uniform flow, then an error-free numerical solution would reproduce that uniform flow; i.e., the computed change in flow variables over a time step would be $\Delta q = 0$. For a flow in which the initial values q^n, f^n, etc., are spatially uniform, the term on the right of Eq. (24a) becomes

$$\begin{aligned}
r = q^n[\Delta J + \Delta\tau(\partial_\xi\hat{\xi}_t + \partial_\eta\hat{\eta}_t + \partial_\zeta\hat{\zeta}_t)] + \Delta\tau f^n[\partial_\xi\hat{\xi}_x \\
+ \partial_\eta\hat{\eta}_x + \partial_\zeta\hat{\zeta}_x] + \Delta\tau g^n[\partial_\xi\hat{\xi}_y + \partial_\eta\hat{\eta}_y + \partial_\zeta\hat{\zeta}_y] \\
+ \Delta\tau h^n[\partial_\xi\hat{\xi}_z + \partial_\eta\hat{\eta}_z + \partial_\zeta\hat{\zeta}_z]
\end{aligned} \tag{25}$$

The last three bracketed terms in Eq. (25) are identical to those in Eq. (11) and vanish analytically, as mentioned earlier. Pulliam and Steger[14] have pointed out that one should employ spatial difference operators that cause these terms to vanish numerically. For a fixed grid, the first bracketed term in Eq. (25) is identically zero. Equation (25) then reduces to $r = 0$ and the operator sequence of Eq. (24) correctly yields the unique solution $\Delta q = 0$. For a moving grid, the correct solution is obtained only if the discretized GCL in Eq. (22) is satisfied numerically, otherwise the solution Δq is in error. One can see that a similar grid motion-induced error would arise in a general nonuniform flow unless the GCL is used to compute J.

To solve Eq. (24), we construct a uniform grid ξ_j, η_k, ζ_l of spacing $\Delta\xi$, $\Delta\eta$, $\Delta\zeta$. We employ second-order central spatial difference operators to evaluate all spatial derivatives:

$$\partial_\xi\alpha = (\alpha_{j+\frac{1}{2},k,l} - \alpha_{j-\frac{1}{2},k,l})/\Delta\xi \tag{26a}$$

$$\alpha_{j+\frac{1}{2},k,l} = (\alpha_{j,k,l} + \alpha_{j+1,k,l})/2 \tag{26b}$$

Equation (26) is equivalent to the classical central difference operator $\mu\delta$.

Pulliam and Steger[14] have shown that when such central difference operators are used to evaluate the metric coefficients of Eq. (19), errors are incurred because the last three bracketed terms in Eq. (25) do not vanish numerically. Those authors present complicated averaging formulas for the metrics that eliminate this source of error. The same end is

achieved with the central difference operators if Eqs. (19) are first rewritten in the conservative form

$$\hat{\xi}_x = (y_\eta z)_\zeta - (y_\zeta z)_\eta \qquad \hat{\eta}_x = (y_\zeta z)_\xi - (y_\xi z)_\zeta$$

$$\hat{\zeta}_x = (y_\xi z)_\eta - (y_\eta z)_\xi \qquad \text{etc.} \tag{27}$$

One can verify easily that the last three bracketed terms in Eq. (25) vanish identically when central difference operators are used to evaluate the spatial derivatives in Eqs. (27).

Relation of the Present Method to the Finite-Volume Method

We now demonstrate that the use of central difference operators in Eq. (24) yields difference equations that are identical to those obtained by applying the finite-volume method in the ξ,η,ζ computational space. The half-integer subscripts in Eq. (26) effectively define the faces of a rectangular volume element that encloses each interior grid point of the computational space (Fig. 1). In the finite-volume method, one integrates Eq. (20) over the cell volume $\mathcal{V}_{jkl} = \Delta\xi\Delta\eta\Delta\zeta$ to obtain

$$\mathcal{V}_{jkl}^{-1}\int_{\mathcal{V}_{jkl}} \Delta\hat{q}\,d\xi d\eta d\zeta = \Delta\tau[(\hat{f}_{j+\frac{1}{2}} - \hat{f}_{j-\frac{1}{2}})/\Delta\xi$$

$$+ (\hat{g}_{k+\frac{1}{2}} - \hat{g}_{k-\frac{1}{2}})/\Delta\eta + (\hat{h}_{l+\frac{1}{2}} - \hat{h}_{l-\frac{1}{2}})/\Delta\zeta]^{n+1} = 0$$

The first term represents the cell-averaged value $\Delta\hat{q}_{jkl}$ at the cell centroid, which coincides with the grid point (j,k,l). Upon linearizing the equation in time and factoring the implicit operator, the resulting "finite-volume" sequence is identical to the "finite-difference" sequence obtained from Eq. (24) by using the central spatial difference operators. Thus, for second-order central difference algorithms, the present finite-difference method is equivalent to applying the finite-volume method in the computational space rather than in physical space, and the GCL provides the means for computing the corresponding physical volume element J in a self-consistent fashion. The present method is superior to the usual finite-difference method in the latter respect. It is also superior to the usual finite-volume method in two ways. First, no external geometric constructions are needed to compute either cell volumes or surface areas and spatial orientations of cell faces. Second, the usual finite-volume method apparently has been attempted with only first- or second-order spatial accuracy, and it is difficult to envision how it might be extended to higher order, in view of its reliance on geometrical constructions. In contrast, the present method is based directly on the set of partial differential equations (12) and (14). In principle, the latter may be discretized to any order of accuracy by the use of appropriate spatial difference operators.

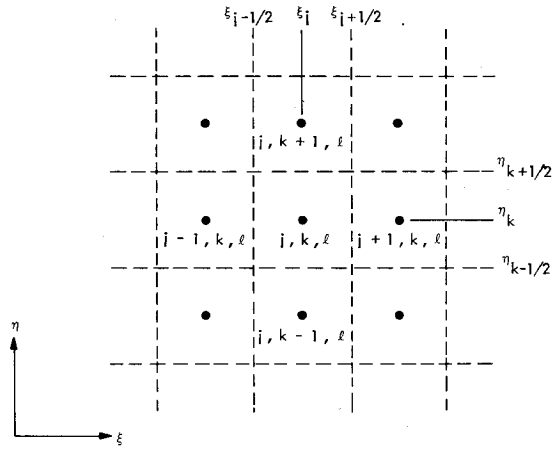

Fig. 1 Sketch of computational grid in a plane ζ = const.

Global Conservation

For accuracy, the finite-difference representation ought to possess the same property of global conservation as the differential equations. The global conservation property of the differential equations spanning the solution domain R is that only the boundary fluxes contribute to the volume integral of the physical variables. For the difference equations, the volume integral is naturally expressed as a quadrature sum. When the difference equations are summed with the appropriate weights of the quadrature, global conservation is achieved for the system if the physical flux makes a net contribution only at the boundaries. As an illustration, consider the one-dimensional case of Eqs. (14) and (24) under the transformation $\xi = x$ on the unit interval:

$$q_\tau + f_\xi = 0, \quad 0 \le \xi \le 1 \tag{28}$$

$$(I + a\mu_j\delta_j F^n)\Delta q = -a\mu_j\delta_j f^n, \quad a = \Delta\tau/\Delta\xi \tag{29}$$

where we employ the mesh depicted in Fig. 2.

$$\xi_j = (j-1)\Delta\xi, \quad 1 \le j \le M \quad \Delta\xi = 1/(M-1) \tag{30}$$

and where the subscript j in Eq. (29) identifies the classical spatial central difference operator $\mu_j\delta_j$. The global conservation property for Eq. (28) is

$$\frac{d}{d\tau}\int_0^1 q\,d\xi = f(0) - f(1) \tag{31}$$

If the difference equations are to possess the gloval conservation property of the differential equation, then the difference operators employed at boundary grid points must be compatible with the interior point central difference operators in Eq. (29). Within the framework of the present modified finite-volume method, we shall illustrate how one can develop conservative difference operators at an outflow boundary $j = M$. For the half-cell at the outflow boundary in Fig. 2, the natural differencing of the flux term between the faces of the boundary half-cell that is compatible with Eq. (26) for interior cells is

$$f_\xi = (f_j - f_{j-\frac{1}{2}})/(\Delta\xi/2), \quad j = M$$

In view of Eq. (26b), this is equivalent to the classical first-order backward difference operator, $\nabla_j f/\Delta\xi$. Upon using this same differencing for the implicit flux term $F\Delta q$, one obtains the following difference equation for the boundary half-cell

$$\Delta q_* + a\nabla_j(F^n\Delta q) = -a\nabla_j f^n, \quad j = M \tag{32}$$

where Δq_* represents the mean value of Δq, averaged over the volume of the half-cell; its proper location is at the centroid of the half-cell (denoted by the asterisk in Fig. 2) rather than at the grid point $j = M$ itself. If one were to assign the value Δq_* to the boundary point as is usually done in the finite-difference method, $\Delta q_* = \Delta q_M$, then the system of difference equations would be only zero-order accurate at the boundary.

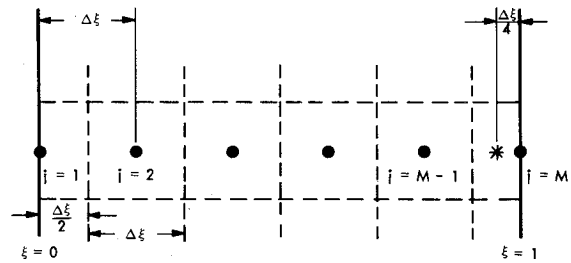

Fig. 2 Finite-difference mesh [Eq. (30)].

This defect can be remedied by linear interpolation of data between the centroid of the last interior cell and boundary

$$\Delta q_* = (3\Delta q_M + \Delta q_{M-1})/4$$

so that Eq. (32) becomes

$$\{I + a\nabla_j[F^n - (1/4a)I]\}\Delta q = -a\nabla_j f^n, \quad j = M \qquad (33)$$

It is easy to show that the difference equations retain the global conservation property of the differential equation. For example, if the boundary half-cell $j=1$ is treated as above, then the weighted sum of the difference equations becomes identical to Eq. (30) to within the implicit linearization of the flux terms $f^{n+1} = f^n + F^n\Delta q$ when the weights are chosen according to the midpoint quadrature rule for discretizing the integral in Eq. (31). The midpoint rule is consistent with the spatial order of accuracy of the difference operators in Eq. (29).

Unsteady Implicit Solutions for Viscous Flow

The formulation described above has been implemented in two and three dimensions through modification of codes of Kutler et al.[2] and Pulliam,[14] respectively, both of which are similar in structure to the original code of Steger.[4] To date, the modified codes have been used in studies aimed ultimately at solving the problem of viscous, hypersonic flow about blunted cones at high angle of attack. The two-dimensional code is an axisymmetric flow version of the three-dimensional code, and has been used extensively in comparatively inexpensive development studies. Both codes feature body normal curvilinar coordinate meshes stretched between body and shock as decribed by Kutler et al.,[2] and make use of the implicit outflow boundary scheme described earlier.

Because the codes are intended to embrace bona fide low Reynolds number thick shock situations, we have developed a scheme that combines the best features of fitting and of capturing the shock in the mesh. The method makes use of the observation by MacCormack[5] that a shock jump may be recovered most accurately in a minimum number of mesh points when the coordinate mesh is aligned with the shock. In our scheme, we apply the freestream conditions to a coordinate surface of mesh points just outside the shock and cross the shock with the numerical method. The grid point velocities in Eq. (21) are computed from the peak recovered pressure according to the method described by Thomas et al.[1] and cause the grid to move toward an equilibrium position that is aligned with the shock.

Figure 3 shows a comparison of drag computed with our two-dimensional axisymmetric code against some experimental values for a short sphere-cone. A calculation of drag from a preliminary three-dimensional solution for the same body at 30 deg angle of attack at a freestream Mach number of 10 and Reynolds number of 1000 showed similar agreement with experiment. Some details of the 30-deg angle-of-attack solution are discussed in the following.

The mesh configuration in the symmetry plane is shown in Fig. 4. Figure 5 shows a projection of the mesh onto a plane normal to the body axis. The grid points beyond the symmetry plane (angle-of-attack plane) are used for convenience in applying symmetry boundary conditions.

Figure 6 shows the computed pressure on the body in the windward and leeward symmetry planes, and in a plane midway between. The pressures, plotted vs running distance

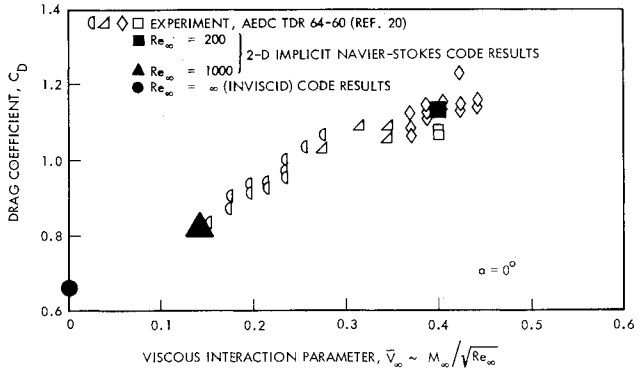

Fig. 3 Implicit two-dimensional unsteady Navier-Stokes code predictions of drag for a blunt 10-deg cone at Mach 10 for several Reynolds numbers. Inviscid drag computation by the method of Sec. IV.

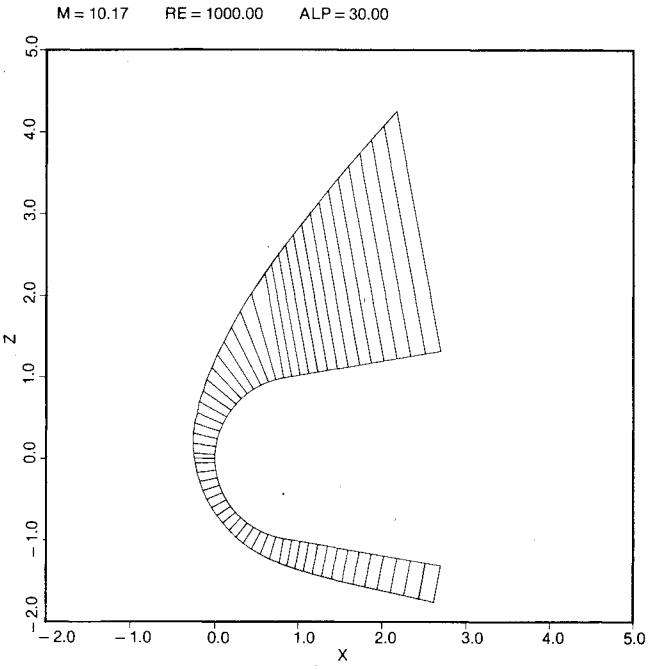

Fig. 4 Body and freestream boundary intersection contours and body normal grid lines in the angle-of-attack plane (symmetry plane).

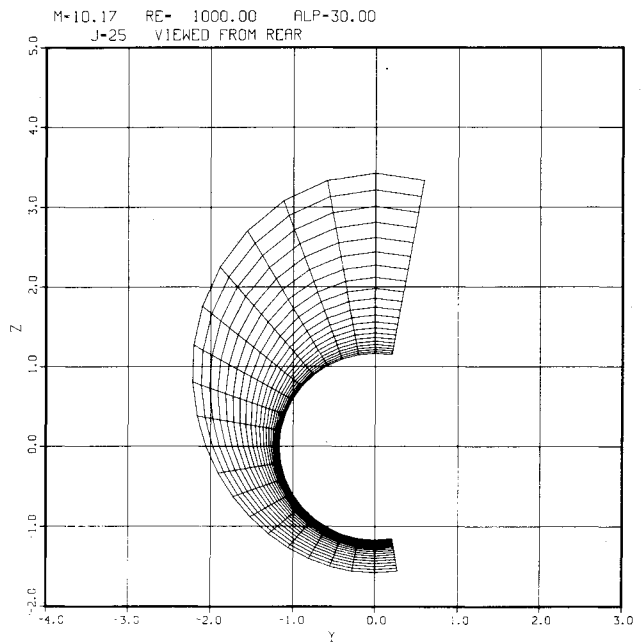

Fig. 5 Crossflow plane section of the computational mesh at a streamwise station located on the conical body section.

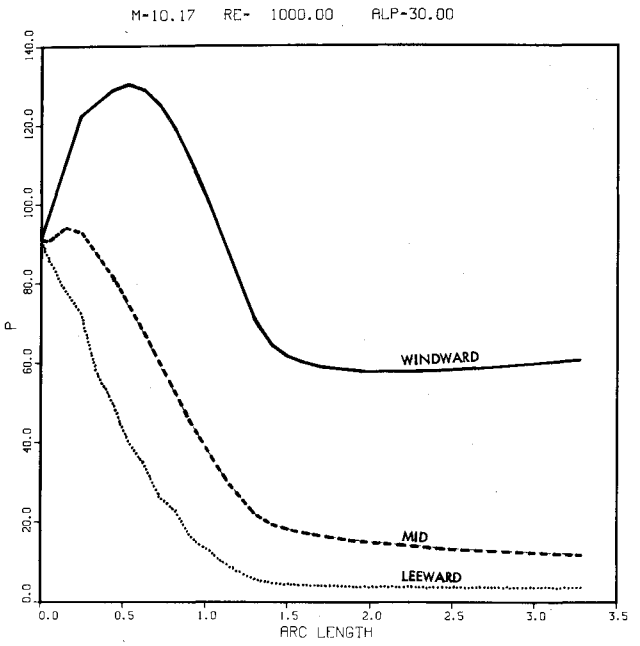

Fig. 6 Pressure profiles along the body in windward and leeward symmetry plane and a midplane.

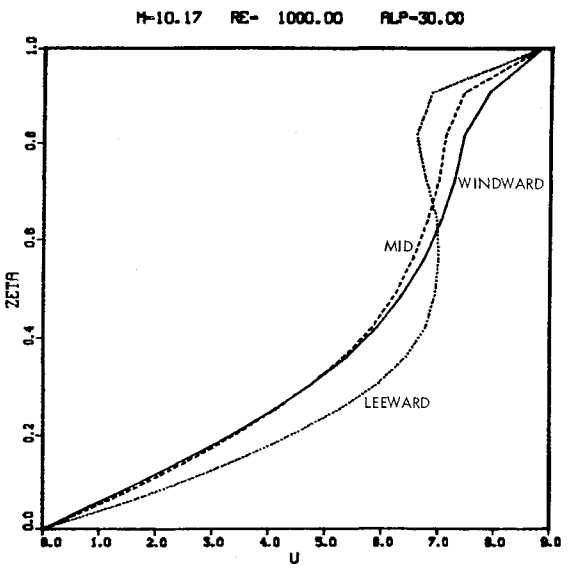

Fig. 7 Profiles of axial velocity component across shock layer in the windward, mid, and leeward planes for a streamwise station about midway along the conical afterbody.

along the body from the nose, are referenced to the freestream pressure.

Figure 7 shows profiles of axial velocity vs ZETA, the shock layer thickness-normalized distance from the body along a body normal coordinate line. The profiles shown are in the windward, mid, and leeward planes at a streamwise station about midway down the conical body section. More comprehensive numerical results from this three-dimensional solution can be found in Ref. 10.

IV. Explicit Solutions for Steady Inviscid Supersonic Flow

Finite-difference solutions for three-dimensional external flows in cylindrical coordinates have been presented by Thomas et al.,[1] who used the nonconservative form of the inviscid Euler equations; and by Kutler et al.,[15] who used a

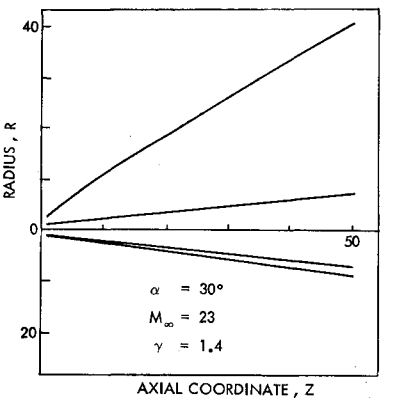

Fig. 8 Body shape and computed shock shape in plane of symmetry for a blunt slender cone. Dimensions are in units of nose radius.

weak conservation form of the equations. Both of these works used MacCormack's original unsplit differencing scheme[11] to integrate the equations forward in the axial direction. A similar problem for reacting flow was treated by Rizzi and Bailey,[7] who used the finite-volume method with the split-operator version of MacCormack's scheme.[5] We present below some solutions to Eq. (16) for three-dimensional external flows and for axisymmetric jet flows using the modified finite-volume method based on the GCL Eq. (18). Space limitations permit only a sampling of results to be presented here. More comprehensive numerical results for the cases described below can be found in Ref. 10.

Three-Dimensional External Flow

For three-dimensional supersonic flow over blunt-nosed bodies, the flow region R downstream of an initial data plane $z=$const. is bounded by a free shockwave surface $r=s\ (\phi,z)$ and the body surface $r=b\ (\phi,z)$. For bilaterally symmetric bodies, it is sufficient to employ the simple transformation

$$X=(r-b)/(s-b), \quad Y=\phi/\pi$$

Equations (16) are solved on a uniform grid using MacCormack's predictor-corrector differencing scheme.[11] The two GCL's, one for the ϕ-momentum equation and the other for the remaining equations, are solved in a similar fashion. One can show that the analogs of the last three bracketed quantities in Eq. (25) vanish numerically if the X and Y derivatives in Eq. (17) are evaluated by the same alternated forward and backward difference formulas used in the MacCormack scheme for Eq. (16) and for the two GCL's.

Symmetry boundary conditions are imposed at the planes $Y=0$, 1. The flow variables at grid points on the body surface are computed using a modification of Kentzer's scheme,[17] which involves the discretized form of a characteristic equation. The bow shock geometry and the flow variables at grid points on the shock surface $X=1$ are computed using a modified version of the method of Thomas et al.[1] The original method employed a central difference formula to evaluate the derivative $s_\phi = Y_\phi s_Y$. This procedure yields good results at moderate angles of attack, but inadequately damps short wavelength circumferential oscillations (wavelength $2\Delta Y$) at high angles of attack where supersonic crossflows develop.[18] The oscillations are eliminated by using the central difference formula only at points near the symmetry planes; at other points, s_Y is evaluated by alternating forward and backward difference formulas between predictor and corrector.

Figure 8 shows the body shape and the computed shock shape in the symmetry plane for a spherically blunted slender cone at 30-deg angle of attack in a Mach 23 freestream. The coordinates shown are normalized by the body nose radius.

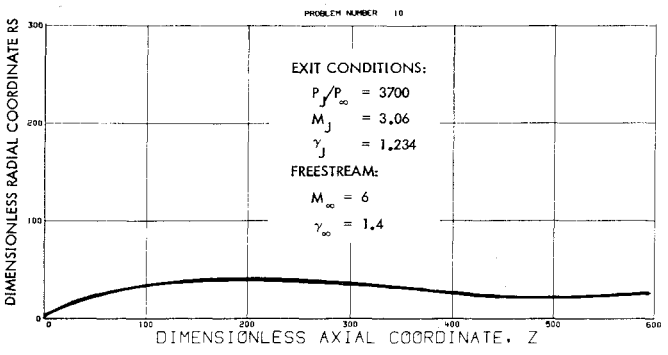

Fig. 9 Computed shape of jet boundary (contact surface) as a function of axial position.

The initial data in a plane normal to the body axis and passing through the sphere-cone juncture were obtained as described by Thomas et al.[1]

Axisymmetric Jets

The axisymmetric flow equations can be obtained from Eqs. (16) and (18) by setting $v=\partial/\partial Y=0$. These equations have been solved for supersonic freejets in which the lower computational boundary is the symmetry axis $r=0$ and the upper boundary is a contact surface $r=r_s(z)$ along which is prescribed a modified tangent-wedge boundary condition[19] that relates the external pressure to the local slope dr_s/dz.

Numerical solutions were obtained with the variant of MacCormack's scheme that employs backward differences in the predictor and forward differences in the corrector, because the reverse scheme proved to be unstable in the strongly expanding flows that arise for high jet exit-to-freestream pressure ratios $p_j/p_\infty \gg 1$. Figure 9 shows the computed shape of the jet boundary for a highly underexpanded jet $p_j/p_\infty = 3700$. Distances shown are normalized by the jet exit radius.

Acknowledgment

This work was supported by the Lockheed Independent Research Program.

References

[1] Thomas, P.D., Vinokur, M., Bastianon, R. A., and Conti, R. J., "Numerical Solution for Three-Dimensional Inviscid Supersonic Flow," *AIAA Journal*, Vol. 10, July 1972, pp. 887-894.

[2] Kutler, P., Chakravarthy, S. R., and Lombard, C. K., "Supersonic Flow Over Ablated Nosetips Using an Unsteady Implicit Numerical Procedure," AIAA Paper 78-213, 1978.

[3] Viviand, H. and Ghazzi, W., "Numerical Solution of the Compressible Navier-Stokes Equation at High Reynolds Numbers with Applications to the Blunt Body Problem," *Lecture Notes in Physics*, No. 59, Springer-Verlag, 1976.

[4] Steger, J. L., "Implicit Finite Difference Simulation of Flow About Arbitrary Geometries with Applications to Airfoils," *AIAA Journal*, Vol. 16, July 1978, pp. 687-692.

[5] MacCormack, R. W. and Paullay, A. J., "The Influence of the Computational Mesh on Accuracy for Initial Value Problems with Discontinuous or Non-Unique Solutions," *Computers and Fluids*, Vol. 2, 1974, pp. 339-361.

[6] Rizzi, A. W. and Inouye, M., "Time-Split Finite-Volume Method for Three-Dimensional Blunt-Body Flow," *AIAA Journal*, Vol. 11, Nov. 1973, pp. 1478-1485.

[7] Rizzi, A. W. and Bailey, H. E., "A Generalized Hyperbolic Marching Method for Chemically Reacting 3-D Supersonic Flow Using a Splitting Technique," *AIAA 2nd Computational Fluid Dynamics Conference Proceedings*, 1975, pp. 38-46

[8] Thompson, J. F., Thames, F. C., and Mastin, C. M., "Automatic Numerical Generation of Body-Fitted Curvilinear Coordinate System for Fields Containing any Number of Arbitrary Two-Dimensional Bodies," *Journal of Computational Physics*, Vol. 15, 1974, pp. 299-319.

[9] Peyret, R. and Viviand, H., "Computation of Viscous Compressible Flows Based on the Navier-Stokes Equations," AGARD-AG-212, 1975.

[10] Thomas, P. D. and Lombard, C. K., "The Geometric Conservation Law—A Link Between Finite-Difference and Finite-Volume Methods of Flow Computation on Moving Grids," AIAA Paper 78-1208, 1978.

[11] MacCormack, R. W., "The Effect of Viscosity in Hypervelocity Impact Cratering," AIAA Paper 69-354, 1969.

[12] Beam, R. and Warming, R. F., "An Implicit Factored Scheme for the Compressible Navier-Stokes Equations," *AIAA Journal*, Vol. 16, April 1978, pp. 393-402.

[13] Briley, W. R. and MacDonald, H., "Solution of the Multidimensional Compressible Navier-Stokes Equations by a Generalized Implicit Method," *Journal of Computational Physics*, Vol. 24, 1977, pp. 372-397.

[14] Pulliam, T. H. and Steger, J. L., "On Implicit Finite-Difference Simulations of Three-Dimensional Flow," AIAA Paper 78-10, Jan. 1978.

[15] Kutler, P., Reinhardt, W. A., and Warming, R. F., "Numerical Computation of Multishocked, Three-Dimensional Supersonic Flow Fields with Real Gas Effects," AIAA Paper 72-702, June 1972.

[16] Vinokur, M., "Conservation Equations of Gasdynamics in Curvilinear Coordinate Systems," *Journal of Computational Physics*, Vol. 14, 1974, pp. 105-125.

[17] Kentzer, C. P., "Discretization of Boundary Conditions on Moving Discontinuities," *Lecture Notes in Physics*, No. 8, Springer-Verlag, Sept. 1970.

[18] Solomon, J. M., Ciment, M., Ferguson, R. E., and Bell, J. R., "Inviscid Flowfield Calculations for Reentry Vehicles with Control Surfaces," *AIAA Journal*, Vol. 15, Dec. 1977, pp. 1742-1749.

[19] Hoshizaki, H., Chou, Y. S., Meyer, J. W., Wilson, K. H., and Thomas, P. D., "Plume Visibility Detection Study," *Proceedings of the JANNAF 10th Plume Technology Meeting*, Vol. 2, Sept. 1977, pp. 21-62.

[20] Boylan, D. E. and Sims, W. H., "Experimental Determination of Aerodynamic Drag on a Blunted 10° Cone at Angle of Attack in Hypersonic Rarified Flow," ARO, Inc., Arnold Air Force Station, Tenn., AEDC-TDR-64-60, 1964.